Surface & Coatings Technology 303 (2016) 319–329

Contents lists available at ScienceDirect

Surface & Coatings Technology

journal homepage: www.elsevier.com/locate/surfcoat

Highly ordered mesoporous silica loaded with dodecylamine for smart anticorrosion coatings

J.M. Falcón [a], L.M. Otubo [b], I.V. Aoki [a,*]

[a] Chemical Engineering Dept., Polytechnic School, University of São Paulo, Brazil
[b] Energy and Nuclear Research Institute, IPEN, São Paulo, Brazil

ARTICLE INFO

Article history:
Received 29 July 2015
Revised 10 October 2015
Accepted in revised form 16 November 2015
Available online 19 November 2015

Keywords:
Nanocontainers
Mesoporous silica
Self-healing coatings
Corrosion inhibitor
Smart coatings
Dodecylamine

ABSTRACT

The development of nanoscience and technology has devoted significant attention to studies on hollow particles. Among these materials, mesoporous silica nanoparticles have recently attracted attention as potential nanocontainers due to their high stability, biocompatibility, large surface area, controllable pore diameter and easy surface functionalization. Mesoporous silica nanoparticles can uptake, store and release organic or inorganic molecules of various sizes, shapes and functionalities. The aim of this work is to study the use of mesoporous silica with hexagonally ordered (4–14 nm) for active corrosion protection of carbon steel. Mesoporous silica was characterized by X-ray diffraction (XRD), nitrogen adsorption isotherms, scanning electron microscopy (SEM) and transmission electron microscopy (TEM). Mesoporous silica structures were loaded with dodecylamine and embedded into an alkyd primer with a weight load ratio of 15 wt.% of mesoporous silica. Kinetics of the release of inhibitor was evaluated by electrochemical impedance measurements in aerated 0.1 mol/L NaCl solution containing 1 wt.% of mesoporous silica at different pH values (2.0, 6.2 and 9.0).

The anticorrosive performance of carbon steel coated with alkyd primer loaded with 15 wt.% of mesoporous silica with entrapped dodecylamine was demonstrated by electrochemical impedance spectroscopy (EIS) and scanning vibrating electrode technique (SVET). Kinetics of inhibitor releasing curves showed that for pH 2.0 condition the release of inhibitor was faster in comparison to other pH conditions (9.0 and 6.2) showing that this complex porous system provides high loading capacity and efficient inhibitor release in low pH. In addition, due to the release of inhibitor during the corrosion process, well-pronounced active anticorrosion properties and self-healing were provided and confirmed by EIS and SVET measurements. Coated samples were also evaluated in a salt spray chamber and the self-healing effect was also remarkable.

1. Introduction

Corrosion protection is a vital concern for hundreds of industrial applications where metals are used as functional and constructional materials [1]. Polymeric coating systems are normally applied on a metal surface to provide a dense barrier against the corrosive species in order to protect metal surfaces from corrosive attack. When the barrier is damaged and the corrosive agents penetrate to the metal surface, the system cannot stop the corrosion process [2]. Recently, a new generation of smart anticorrosion coatings has been proposed and investigated, which are composed of two functional components. One part is passive coatings, such as sol–gel coatings and polymer coatings, which act as a physical barrier against corrosive species [3,4]. The other part is smart nanocontainers, which are uniformly dispersed in the passive coatings and can quickly respond to local environmental changes associated with corrosion processes, such as local pH, ionic strength and potential, and release encapsulated corrosion inhibitors to retard the corrosion process [2,5–9]. Introduction of environmentally friendly corrosion inhibitors for protective coatings is very important and opportune [10]. A new generation of ordered mesoporous materials, making a subclass of nanoporous materials, has become a challenge of great interest. Since the beginning of 1990s, when the workers of Mobil Co. (USA) [11] reported the method of synthesis of mesoporous materials employing surfactants as structurally ordering agents, the importance of these materials has considerably increased. Because of large internal and external surface area, they have been indicated as potential carriers for therapeutically active substances allowing controlled release of the drug. Moreover, the size of mesopores can be regulated by the proper choice of the precursors [12–14]. Mesoporous materials based on silica show low toxicity (are practically nontoxic), low reactivity and can be modified to get the channel size and shape suitable for adsorption of large molecules of active substances [15–16]. A highly ordered mesoporous silica was synthesized using tri-block copolymer poly(ethylene oxide)–poly(propylene oxide)–poly(ethylene oxide) surfactant, which is commercially available as Pluronic P123 ($EO_{20}PO_{70}EO_{20}$) [17–21].

* Corresponding author at: Chemical Engineering Dept., Electrochemistry and Corrosion Laboratory, Av. Prof. Luciano Gualberto, Travessa 3, No. 380, São Paulo, SP CEP 05508-010, Brazil.
E-mail address: idavaoki@usp.br (I.V. Aoki).

http://dx.doi.org/10.1016/j.surfcoat.2015.11.029
0257-8972/

This mesoporous silica possess large BET surface area (>700 m^2/g) with large pore diameter and large wall pore thickness. The well-controlled pore size, narrow pore size distribution, controllable functionality and pore surface chemistries of nanoporous silica materials suggest their use as the encapsulating material for controlled release of corrosion inhibitors. These corrosion inhibitors can be encapsulated in such structure in order to be added in a primer to promote a long-term cost-effective protection of a whole coating system [22–26]. Different approaches to encapsulate drugs and corrosion inhibitors within mesoporous materials have been explored and reported in the literature. Kiwilsza et al. [21] synthesized SBA-15 mesoporous silica to be used as a carrier for a poorly soluble drug — lacidipine (LA). The source of silica was tetraethyl orthosilicate (TEOS) and the structure ordering agent was non-ionic surfactant Pluronic P123. SBA-15 with encapsulated LA was characterized by X-ray diffraction (XRD), infrared spectroscopy (FTIR), thermogravimetry (TG), differential scanning calorimetry (DSC) and transmission electron microscopy (TEM). Ordered hexagonal arrangement of synthesized silica and controllable release of encapsulated inhibitor were found. Borisova et al. [24] used mesoporous silica nanoparticles as nanocontainers loaded with 1H-benzotriazole (BTA) and added in hybrid sol–gel coating for the corrosion protection of aluminum alloy. Techniques as N_2 adsorption–desorption isotherms (BET), scanning electron microscopy (SEM) and transmission electron microscopy (TEM) were used for characterizing the synthesized mesoporous silica. The corrosion protection efficiency of coated samples was monitored via SVET (scanning vibrating electrode technique). The anticorrosion performance was improved by impregnating the mesoporous silica loaded with inhibitor into sol–gel coating. Chen and Fu [25] reported the use of benzotriazole-loaded mesoporous silica spheres with pH-sensitive supramolecular nanovalves attached to their surface. The synthesis process of mesoporous silica spheres and the assembly process of the nanovalves were confirmed by adsorption–desorption isotherms (BET), scanning electron microscopy (SEM) and transmission electron microscopy (TEM), Fourier transform infrared spectroscopy (FTIR) and thermogravimetry (TGA). The results showed that the release rate of corrosion inhibitor was higher in alkaline solution than in neutral solution. Gonzales et al. [27] developed the use of SBA-15 mesoporous silica nanoparticles as nanocontainers for $Fe(NO_3)_3$ corrosion inhibitor. Mesoporous silica nanoparticles were mixed with the paint at different concentrations to study their performance and ensure their free transportation to the exposed metal. Steel samples were coated with inhibitor silica nanocontainer doped paint and immersed in an aqueous solution of 3% sodium chloride. Polarization curves and electrochemical noise techniques were used to evaluate the corrosion inhibitor system behavior. Good performance was obtained in comparison with samples without inhibitor nanocontainers. The use of inhibitors encapsulated in mesoporous silica particles is still in its beginning but it is undoubtedly a promising approach. Another aspect of this recent technology, not very explored until now, is the use of encapsulated amines in mesoporous oxides, sensitive to different stimulus and able to increase the anticorrosive properties of alkyd primers. This aspect is explored in this work, where the self-healing effect of alkyd primer coatings doped with dodecylamine-loaded mesoporous silica was evaluated by the use of electrochemical techniques as EIS and SVET and salt spray chamber accelerated corrosion test.

2. Experimental

2.1. Materials

Plates of AISI 1020 carbon steel were used in this study which were previously treated with CSi emery papers from 120 to 600 grit, sequentially, and then rinsed with distilled water, alcohol and acetone. Samples were cut in different dimensions depending on the specific test. Pluronic (P123, $EO_{20}PO_{70}EO_{20}$) was purchased from Sigma Aldrich (St. Louis, MO, USA). Tetraethylortosilicate (TEOS, 97%) was obtained from Momentive Performance Coatings (Brazil). All reagents are of analytical grade purity.

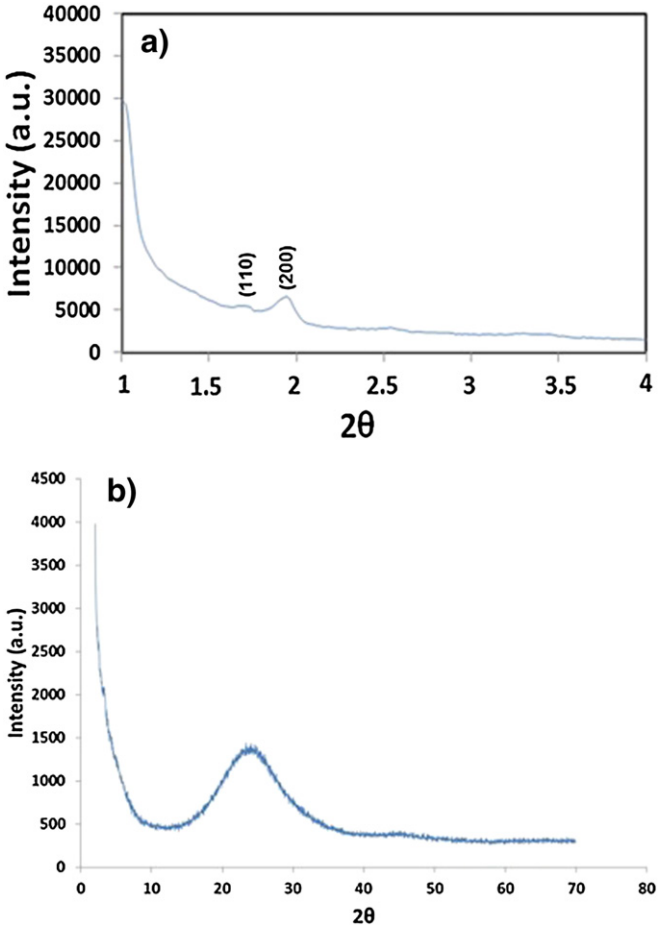

Fig. 1. Powder XRD patterns of calcined mesoporous silica at small 2θ angles (a) and high 2θ angles (b).

2.2. Synthesis of mesoporous silica

Mesoporous silica was synthesized as reported by Zhao et al. [17] using Pluronic P123 triblock copolymer ($EO_{20}PO_{70}EO_{20}$). A 4.0 g sample

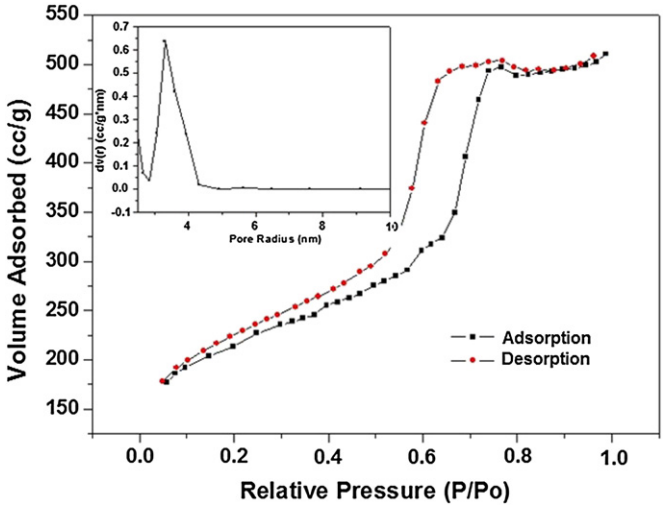

Fig. 2. Nitrogen adsorption–desorption isotherm plots and pore size distribution curve for calcined mesoporous silica.

of Pluronic P123 was dissolved in 130 ml of water and 20 ml of 2 mol/l HCl solution. Then, 9.14 ml of TEOS was added, and the resulting mixture was stirred for 7.5 h at 45 °C and then kept at 80 °C for 15.5 h without stirring. The solid product was washed and filtered with distilled water repeatedly (four times) and dried at room temperature. The removal of organic surfactant was achieved by calcination in ambient air from room temperature to 550 °C, with a heating rate of 1 °C/min, and a holding time of 6 h at 550 °C. Cooling down was performed naturally.

2.3. Characterization of mesoporous silica

XRD measurements of the powdered samples were performed using a Panalytical X'Pert diffractometer using Cu Kα radiation, tube power 40 kV, 40 mA at room temperature. The angle measurements were performed in the range $2\theta = 0.96°$ to 80° with a step of 0.02°.

The BET adsorption/desorption isotherm was determined by nitrogen sorption at 77 K using a Quantachrome NOVA-2000 instrument. The total pore volume was determined from the adsorption branch of the N_2 isotherm curve at a relative pressure of $p/p = 0.98$. A standard isotherm was obtained with 80 data points. For the calculation of the surface area, a nitrogen cross section of 16.2 $Å^2$ was used. The most frequent diameter of pores (mode of pore diameter distribution) was calculated by two different methods: the BJH method (Barrety–Joyner–Halenda), applied to the desorption branch of isotherm, and the DFT method (density functional theory) using a routine available in the Quantachrome NovaWin software version 11.02 of Quantachrome equipment that was developed for the adsorption of N_2 on porous materials based on silicon, assuming a cylindrical pore model.

SEM was performed on a TESCAN VEGA 3 LMU scanning electron microscope. The samples were prepared by placing mesoporous silica

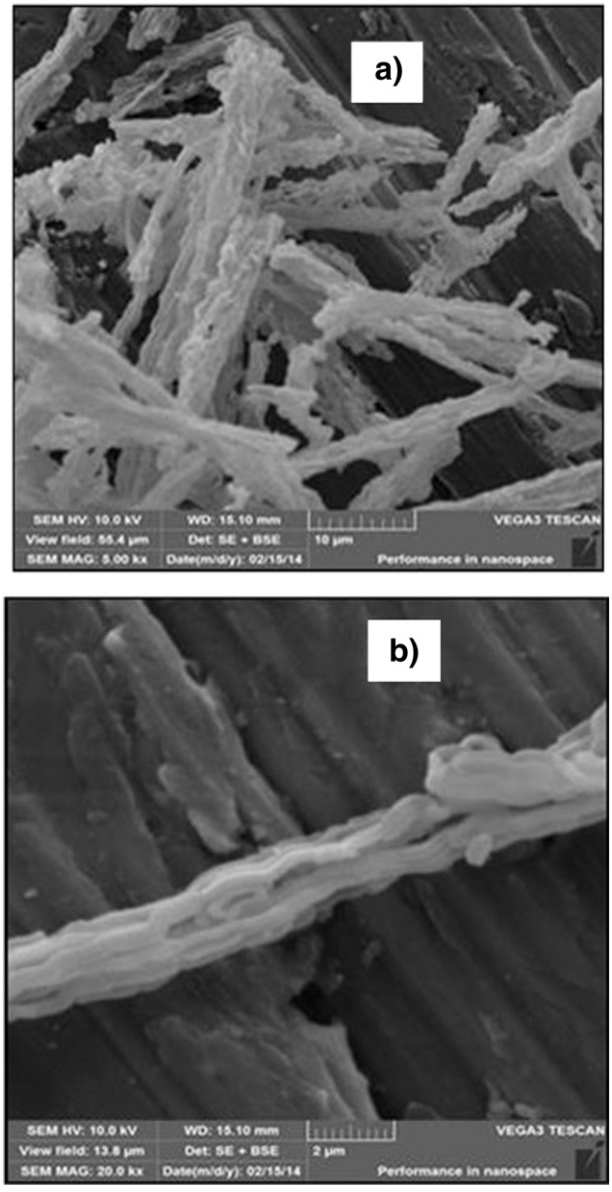

Fig. 3. Scanning electron micrographs of calcined mesoporous silica for different magnifications (a) 5000× and (b) 20000×.

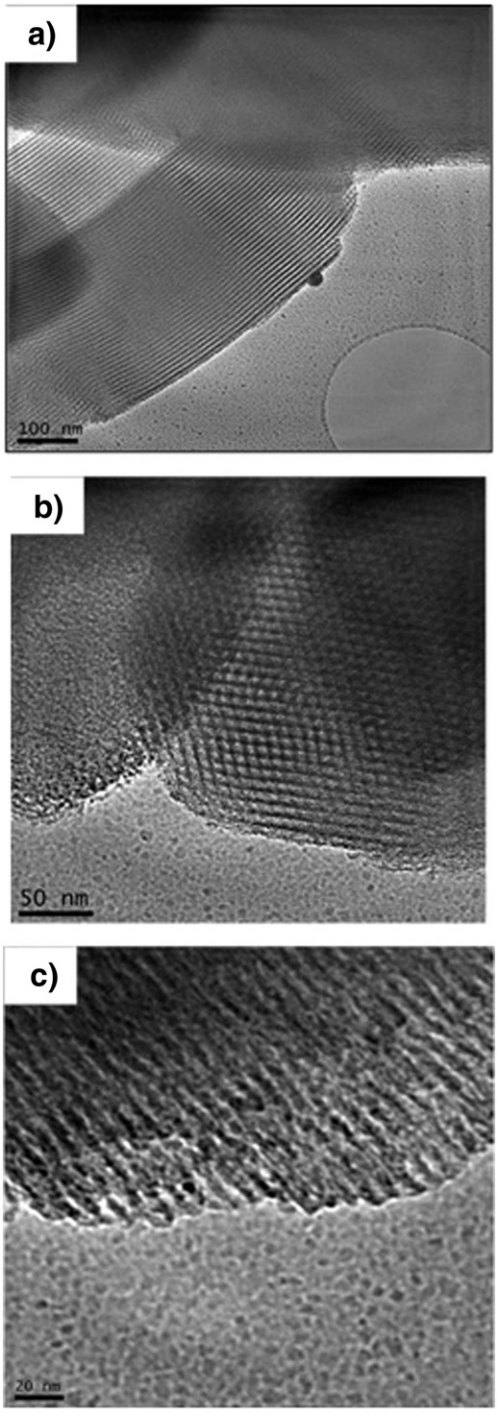

Fig. 4. TEM images of calcined mesoporous silica (a) aligned pore channels and (b, c) entrance of hexagonal pores in the silica fibers walls.

powder on double-sided carbon adhesive tape mounted on the sample holder.

Transmission electron micrographs were obtained using a JEM-2100 made by JEOL Ltd., with an acceleration voltage of 200 kV. The powder samples were mixed in isopropanol and then sonicated for 10 min. A drop of the wet sample was placed on copper grid and allowed to dry for 10 min before TEM analysis.

2.4. Loading, doping and coating

To load the dodecylamine inside the pores of the mesoporous silica an adapted procedure described by Price et al. [28] was performed. In the first step, 6 mL of dodecylamine inhibitor solution with a concentration of 10 mg/mL in ethanol was prepared. In the second step, 50 mg of mesoporous silica was added to the dodecylamine inhibitor solution. The container with the mixture was transferred to a vacuum jar, sonicated for 15 min and then evacuated using a vacuum pump, which deaerates the internal channels of the silica pores. Slight fizzing of the suspension indicates the air being removed from the channels. After fizzing was stopped, the vial was sealed for 30 min to allow dodecylamine reach equilibrium between the inner volume of pores and the surrounding solution. The vacuum treatment was followed by water washing and centrifugation. The supernatant was removed and the precipitate was dried at 60 °C overnight.

Coated samples were obtained by applying the paint with the help of a brush in two layers of approximately 143 μm total dry thickness. A commercial alkyd paint doped with 15 wt.% of dodecylamine-loaded mesoporous silica was prepared to coat (100 mm × 150 mm) panels as a primer (first layer of about 127 μm wet thickness) and a second layer without silica with the same thickness was also applied. Thickness measurements were made using a Fisher Model DualScope® MP40 with a probe based on attenuation of the magnetic field.

2.5. Electrochemical measurements

EIS measurements were employed to evaluate two different types of systems: at first for determining indirectly the release of corrosion inhibitor from mesoporous silica by monitoring the corrosion behavior of carbon steel samples in 0.1 mol/L NaCl solution at different pHs (2.0, 6.2 and 9.0) and containing 1 wt.% of dodecylamine-loaded mesoporous silica and at second, for evaluating the corrosion protection performance of coated samples with alkyd paint doped with dodecylamine-loaded mesoporous silica in 0.01 mol/L NaCl solution. In order to accelerate the corrosion process of these samples a small defect on the coated sample of approximately 130 μm in diameter was made by an indenter just before starting the experiment.

EIS measurements were performed at open circuit potential for different immersion times using a Gamry Reference 600 potentiostat/galvanostat/frequency analyzer and controlled by Gamry Framework software. A frequency range from 50 kHz to 5 mHz with a sinusoidal potential amplitude perturbation of 10 mV rms was adopted.

SVET measurements were performed using the Applicable Electronics equipment controlled by ASET (Sciencewares) software. Samples were prepared for SVET measurements by cutting into 1 × 1 cm^2 area plates. In order to accelerate the corrosion process and evaluate the corrosion resistance of these coated samples, a small scratch of approximately 3 mm in length was made on the coated sample using a sharp

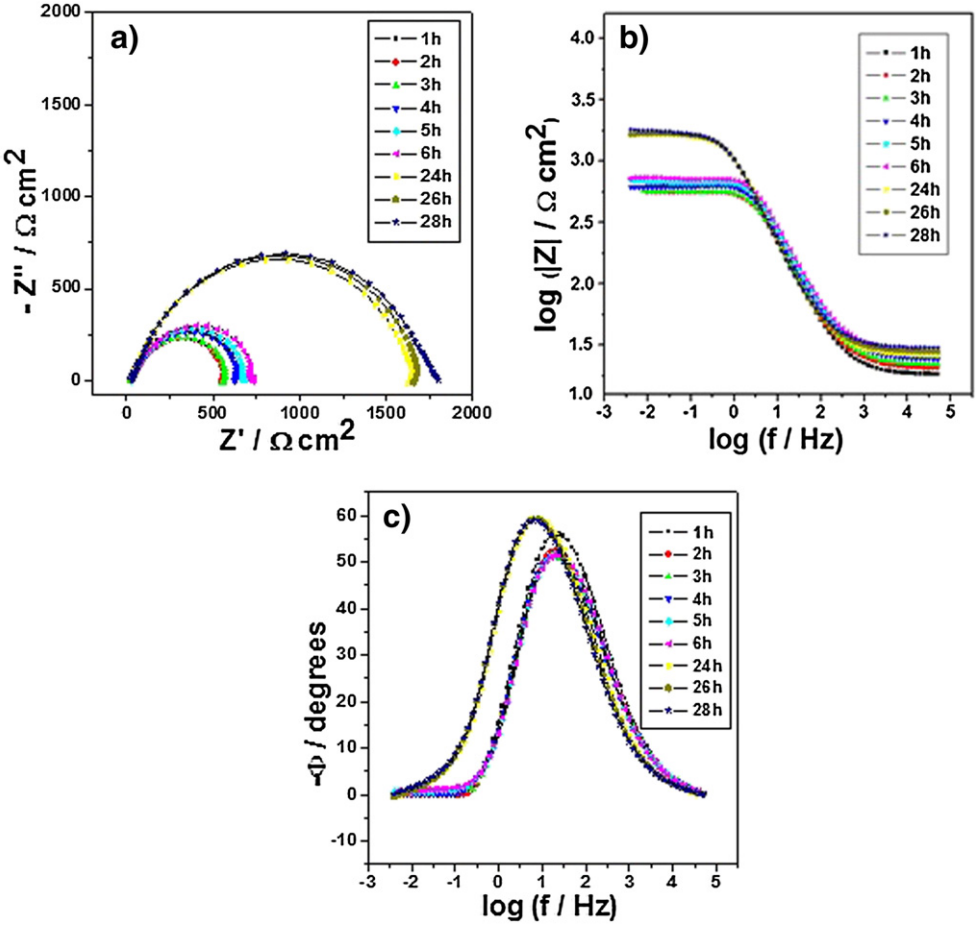

Fig. 5. Impedance diagrams: Nyquist (a) and Bode (b and c) plots for carbon steel after different immersion times in 0.1 mol/L NaCl at pH 2 and containing 1 wt.% of mesoporous silica with encapsulated dodecylamine.

tool. For SVET measurements, a 0.05 mol/L NaCl solution was used as electrolyte.

2.6. Accelerated corrosion test

Salt spray accelerated corrosion experiments were performed by using the equipment Bass Model USC-ISSO-(PLUS), following the recommendations of ASTM B 117-11 Standard. In order to accelerate the corrosion process scratches of 9 cm long were made on the coated samples using a sharp tool before samples entered in the salt spray cabinet.

3. Results and discussions

3.1. Powder X-ray diffraction (XRD)

X-ray diffraction of the calcined sample to identify the structures that characterize this mesoporous silica was performed. Fig. 1a shows the XRD pattern of mesoporous silica, where it is possible to observe three main peaks: the most intense, reaching a maximum at $2\theta = 1.01°$, can be assigned to the (100) plane, the other two corresponding to $2\theta = 1.68°$ and $2\theta = 1.9°$ are assigned to the (110) and (200) planes, respectively. Similar results have been reported by Zhao et al. [17], who were the first to obtain mesoporous silica SBA-15 type with the use of triblock co-polymer (PEO–PPO–PEO) in an acidic environment (pH ~ 1) and by other authors in the literature [18–21]. This silica has no typical crystalline structure and only three peaks appear at very small 2θ angles.

Fig. 1b shows the X-ray diffraction of mesoporous silica for higher 2θ angle values where it is possible to observe a single wide band (no peak) with a maximum for 2θ ~ 25° proving the presence of an amorphous structure typical of such mesoporous silica.

3.2. Nitrogen adsorption

N_2 adsorption–desorption isotherms and pore diameter distributions of the calcined mesoporous silica were also studied (Fig. 2). This mesoporous silica owns typical Type IV isotherm and a clear type-H1 hysteresis loop, which is representative of an adsorbent material with a narrow distribution of relatively uniform pores, further confirming the characteristic of the mesoporous material [29]. Furthermore, from N_2 adsorption–desorption isotherms three well-distinguished regions are evident: (i) monolayer–multilayer adsorption, (ii) capillary condensation, and (iii) multilayer adsorption on the outer particle surfaces. The capillary condensation occurs at higher relative pressure (P/Po ~ 0.75) [17].

By the well-pronounced aspect of the BET isotherm, it is possible to obtain the pore-size distribution (Fig. 2 — inset) which indicates that silica nanomaterial sample has well-defined uniform pore dimensions with an average pore radius size of 2–3 nm.

3.3. Scanning electron microscopy (SEM)

SEM images reveal that mesoporous silica showed in Fig. 3a consists of many rope-like domains with relatively uniform sizes. This large fibrous structure of 20–30 μm in length and 3–5 μm in diameter is an

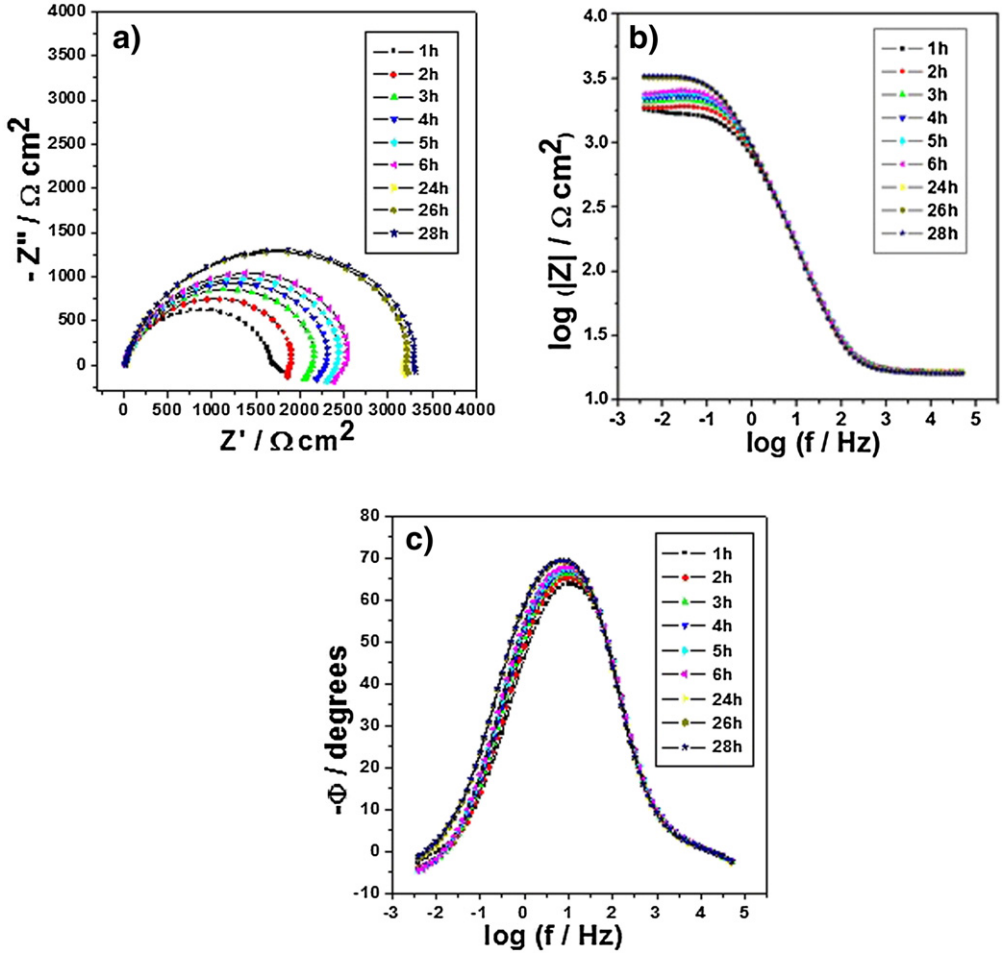

Fig. 6. Impedance diagrams: Nyquist (a) and Bode (b and c) plots for carbon steel after different immersion times in 0.1 mol/l NaCl at pH 6.2 and containing 1 wt.% of mesoporous silica with encapsulated dodecylamine.

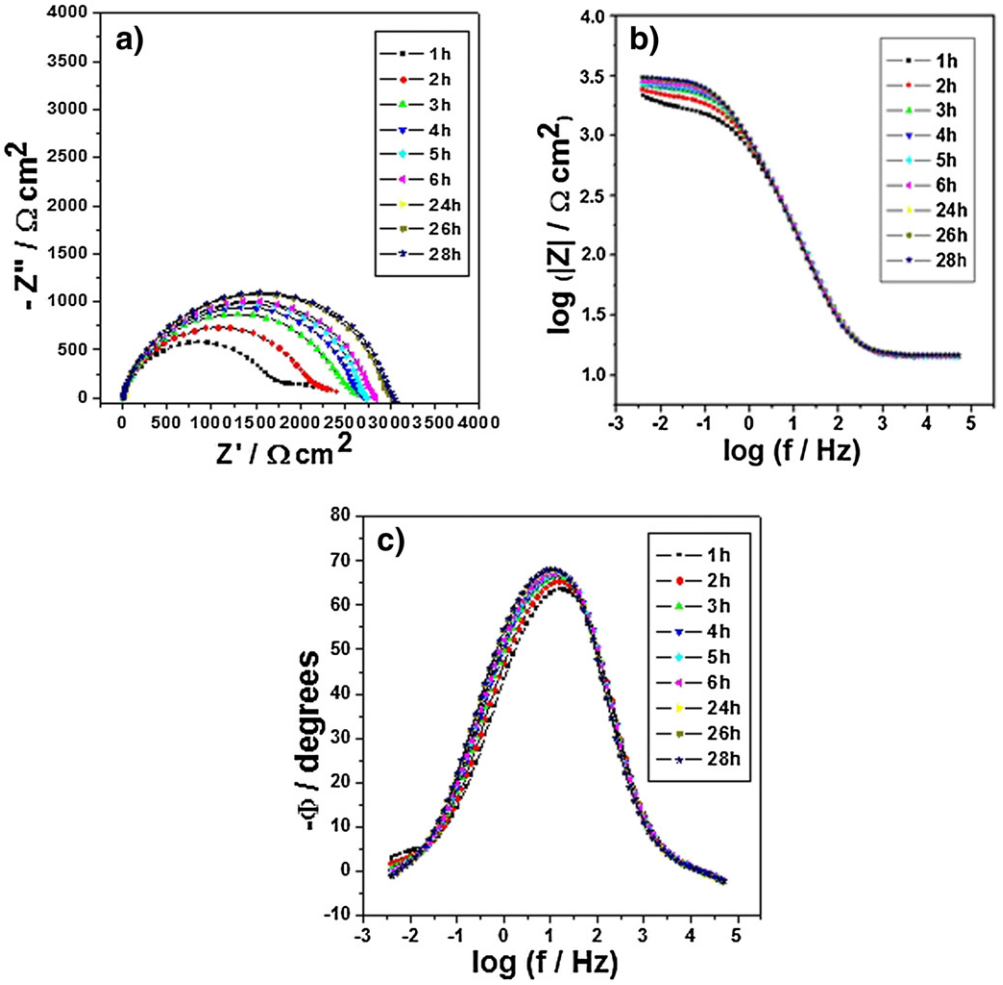

Fig. 7. Impedance diagrams: Nyquist (a) and Bode (b and c) plots for carbon steel after different immersion times in 0.1 mol/l NaCl at pH 9 and containing 1 wt.% of mesoporous silica with encapsulated dodecylamine.

agglomerate of long fibers that are constituted of small rod-like subparticles of 1–2 μm in length and 0.5 μm in diameter (Fig. 3b). Similar SEM images were reported in the literature [17,30,31].

3.4. Transmission electron microscopy (TEM)

Transmission electron microscopy (TEM) images of mesoporous silica SBA-15 are presented in Fig. 4. It is possible to observe in Fig. 4a the formation of well-defined parallel channels on the synthesized sample, where the mesopores are uniformly and radially aligned from the center to the outer surface of the mesoporous particles. The TEM images show clearly the well-ordered hexagonal arrangement of mesopores with internal diameter of about 6 nm to 7 nm (Fig. 4b), which are formed on the walls of the silica represented by a 2-D structure. Fig. 4c is a front view of pore entrance in the mesoporous silica fiber walls. These results are in agreement with those obtained by other authors [17,27,30,31], who obtained images with the same characteristics. Thus, the conditions used for obtaining this mesoporous silica with ordered hexagonal arrangement were successfully applied.

3.5. Kinetics of releasing of dodecylamine inhibitor from mesoporous silica for different values of pH

In order to evaluate kinetics of releasing of dodecylamine inhibitor from mesoporous silica, EIS measurements were performed for carbon steel samples in aerated 0.1 mol/L NaCl solution containing 1 wt.% mesoporous silica loaded with dodecylamine inhibitor at different pH values (2.0, 6.2 and 9.0).

Nyquist diagrams in Fig. 5a show that for pH 2.0 condition there was a small increase of the capacitive arc diameter during the first periods of immersion (1 h, 2 h, 3 h, 4 h, 5 h and 6 h). That is, for short increments of immersion time the values of capacitive arcs diameter does not increase

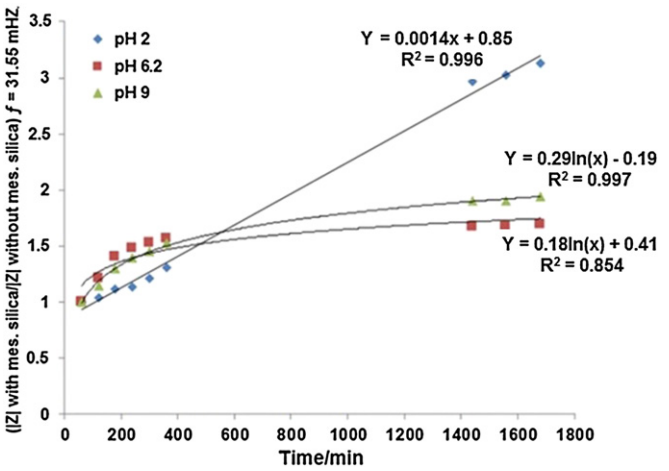

Fig. 8. Kinetics curves for the release of encapsulated dodecylamine inhibitor from mesoporous silica for different immersion times in 0.1 mol/L NaCl solution and different pH values.

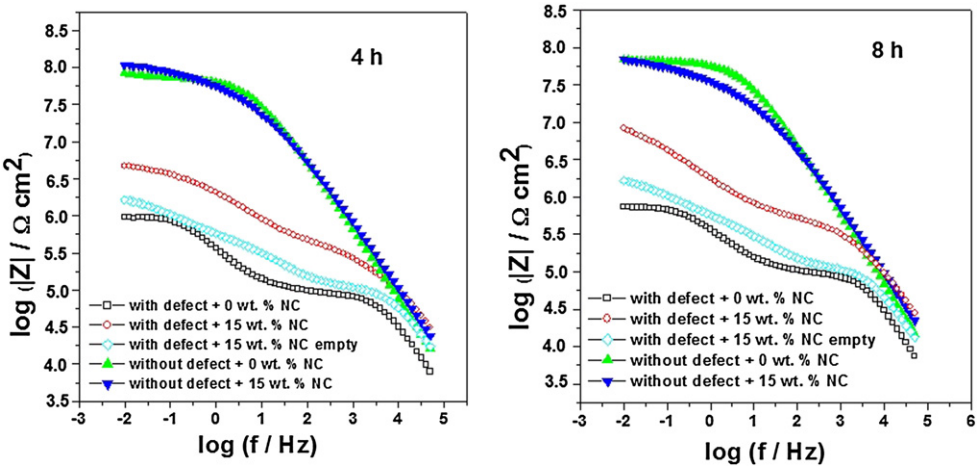

Fig. 9. EIS diagrams: Bode plots for carbon steel coated with alkyd primer doped with 0 wt.% or 15 wt.% of mesoporous silica nanocontainers (NC) loaded or not with dodecylamine obtained after 4 h and 8 h of immersion in 0.01 mol/L NaCl with and without a provoked defect.

significantly reaching a maximum value of 750 Ω cm^2 after 6 h of immersion. In the case of long periods of immersion (24 h, 26 h and 28 h) the capacitive arc diameter increases till reaching a value of almost 2.3 times higher (1750 Ω cm^2) compared with the value obtained for initial immersion times. Changes in the capacitive arcs diameter mean a higher resistance to charge transfer in the metal/electrolyte interface or Faradaic currents. For a bare metal, like carbon steel in this case, higher impedance modulus at lowest frequencies also means a less intense charge transfer in the same metal/electrolyte interface. The presence of a corrosion inhibitor in the electrolyte that is able to adsorb in the metal surface, also slows down the charge transfer process by blocking active sites on the metal's surface, resulting in higher capacitive arc diameters or higher impedance modulus at low frequencies. It is also very important to note that after a visual inspection on carbon steel samples there was no formation of any corrosion products on the metal's surface.

The same behavior was also confirmed by the displacement of phase angle from higher frequencies to lower frequencies in the Bode diagram (θ vs. log f). This characterizes the more protective role of dodecylamine inhibitor released from the mesoporous silica particles over time for carbon steel, which acts forming an adsorbed film on the surface of carbon steel.

Fig. 6 shows the impedance diagrams at pH 6.2 for different immersion times, where one can observe a similar behavior for pH 2 condition. In this case, for initial immersion times the maximum value obtained for 6 h of immersion was around 2250 Ω cm^2. For longer immersion times (24 h, 26 h and 28 h) the capacitive arc diameter reached a value of 3250 Ω cm^2 (1.4 times the initial value), thus, the ratio between impedance modulus in the presence and absence of mesoporous silica particles (|Z| with mesop. silica/|Z| without mesop. silica) was proportionally lower in comparison to pH 2.0 condition.

For pH 9.0 condition shown in Nyquist diagrams (Fig. 7a) it is possible to observe that for long immersion times (24 h, 26 h and 28 h) the increase of capacitive arcs diameter was not significant (1.1 times), even for short periods of immersion (1 h, 2 h, 3 h, 4 h, 5 h and 6 h).

According to the results of kinetics of releasing of dodecylamine inhibitor for different pH conditions it is possible to conclude that for pH 2.0 condition there is a greater amount of released inhibitor from the mesoporous silica. At pH values different from neutral, both silica particles as well as inhibitor molecules have the same charge (positive at pH < 6 and negative at pH > 6). This leads to larger electrostatic repulsion forces and faster release. These results are very favorable for the subsequent application of the loaded silica nanocontainers in anticorrosive active coatings, as the corrosion is usually followed by alkaline or acidic pH shift. Thus, a release of the inhibitor in response to a pH change in the local environment is provided and will be responsible for substrate protection in the coating damaged area [24,32].

Fig. 8 summarizes the linear and logarithmic kinetics for release of encapsulated dodecylamine inhibitor from mesoporous silica for different immersion times in 0.1 mol/L NaCl solution and different pH values. The ratio |Z| with mesop. silica/|Z| without mesop. silica for a fixed frequency of 31.55 mHz was chosen to assess the release of encapsulated corrosion inhibitor. To calculate the impedance module values (|Z| with mesop. silica) for different immersion times it is necessary to find the values of log|Z| with mesop. silica from Bode plots (log (|Z|) vs. log f) for each condition of pH and at a fixed frequency $f = 31.55$ mHZ for different immersion times. This frequency value of 31.55 mHz was chosen due to the fact that at low frequencies it is possible to detect the charge transfer phenomena in the metal/solution interface and consequently the corrosion behavior of the metal immersed in an aggressive medium. For instance, for pH 2 condition, time = 60 min and frequency of 31.55 mHz is obtained a value of $\log|Z|_{t=60\ min} = 2.7988$, then the value of the impedance modulus would be $|Z|_{t=60\ min} = 10^{2.7988} = 553.73$ Ω cm^2. The values of the ratio |Z| with mesop. silica/|Z| without mesop. silica are calculated dividing the values of |Z| with mesop. silica for different immersion times by the |Z| without mesop. silica. This value of |Z| without mesop. silica can be considered as the value of |Z| obtained after 60 min of immersion, since for this short time the action of the corrosion inhibitor is negligible. With these values the kinetic curves for the release of encapsulated dodecylamine inhibitor were obtained plotting the value of (|Z| with mesop. silica/|Z| without mesop. silica) vs. immersion time for each pH condition, shown in Fig. 8.

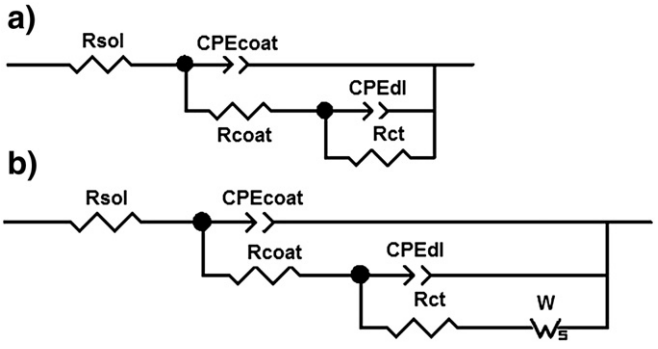

Fig. 10. Equivalent circuit models (ECM) for fitting EIS data for carbon steel coated with alkyd primer doped with 0 wt.% or 15 wt.% of mesoporous silica nanocontainers (NC) after 8 h of immersion in 0.01 mol/L NaCl with a provoked defect. a) The initially used ECM and b) the finally used ECM to fit EIS data.

Table 1
Parameters determined from fitting EIS data to equivalent electric circuit for samples of coated carbon steel with a provoked defect after 8 h of immersion.

ECM parameter		Samples					
		Alkyd primer without NCs	Fitting error (%)	Alkyd primer with empty NCs	Fitting error (%)	Alkyd primer with NCs loaded with inhibitor	Fitting error (%)
R_{sol} (Ω cm^2)	Solution resistance	1258	Fixed	1300	Fixed	1300	Fixed
CPE_{coat} (nF cm^2/S$^{\alpha-1}$)	Capacitance of the alkyd primer coating	0.54	8.68	0.84	3.75	1.23	5.63
CPE_{coat} (α)	Exponent of the CPE coat	0.98	0.74	0.90	0.34	0.81	0.60
R_{coat} (kΩ cm^2)	Resistance of the alkyd primer coating	74.8	4.12	106.5	1.03	415.7	1.58
CPE_{dl} (μF cm^2/S$^{\alpha-1}$)	Double electric layer capacitance	0.62	5.72	0.19	12.51	0.25	1.25
CPE_{dl} (α)	Exponent of the CPE_{dl}	0.48	8.16	0.65	2.84	0.49	1.07
R_{ct} (kΩ cm^2)	Charge transfer resistance	26.8	40.5	292.1	19.16	13,661	3.54
W (kΩ cm^2)	Resistance associated to Warburg element	731.4	3.24	1700.9	7.67	3035.8	66.4
W (α)	Exponent related to Warburg element	0.52	3.05	0.31	4.71	1.0	5.52

For initial immersion times one can observe that the impedance modulus ratio for the three conditions of pH (2.0, 6.2 and 9.0) were very similar, that is, the release rates of dodecylamine inhibitor was not significantly altered by the variation of pH. On the other hand, for longer immersion times the impedance modulus ratio variation with time follows different mathematical models (linear for pH 2.0 and logarithmic for pH 6.2 and 9.0). The global classification of kinetics of inhibitor release is pH 2.0 > pH 9.0 > pH 6.2 explained by the electrostatic interactions mentioned above. In conclusion, for pH 2.0 the rate of release of the inhibitor is the highest in comparison to the rates obtained for pH 6.2 and pH 9.0.

3.6. Self-healing effect for coated samples by EIS and SVET

3.6.1. EIS measurements

The Bode diagrams (log |Z| vs. log f) corresponding to the coated samples with two layers of alkyd paint and the primer containing 0 wt.% or 15 wt.% are presented in Fig. 9a and b. It can be seen that initially (4 h of immersion) the addition of 15 wt.% of mesoporous silica did not affect the performance of the coating due to the fact that the impedance modulus values are very close at low frequencies [33]. After 8 h of immersion, there was a slight decrease in the value of the impedance modulus for the samples without defect and containing 15 wt.% of mesoporous silica due to the ingress of the electrolyte through the pathways or pores formed in the coating, but without affecting the global coating performance. In the case of defective coatings for both immersion times (1 h and 8 h), the samples containing dodecylamine-loaded mesoporous silica exhibit impedance values and phase angles higher in comparison with the samples without mesoporous silica, and this effect is more pronounced after a longer immersion time (8 h). This occurs as consequence of the release of the inhibitor from the internal channels of the mesoporous silica on the defect area. Other authors found similar results [23,24]. In addition, these high impedance modulus values at high and low frequencies are related to best barrier properties and a higher metal polarization resistance due to the presence of inhibitor, respectively [4,34]. In the case of the defective samples containing mesoporous silica without inhibitor a slight increase of the impedance module values at high and low frequencies can also be observed in comparison with the coated samples with pure alkyd primer. A possible explanation is that the empty mesoporous silica particles act as an inorganic and inert charge normally added to paints to improve their barrier properties.

The impedance plots can be utilized to provide adequate modeling of the physicochemical process on the coated sample during corrosion tests. For quantitative information from EIS technique, data were fitted using equivalent electric circuits. In these equivalent circuits, the

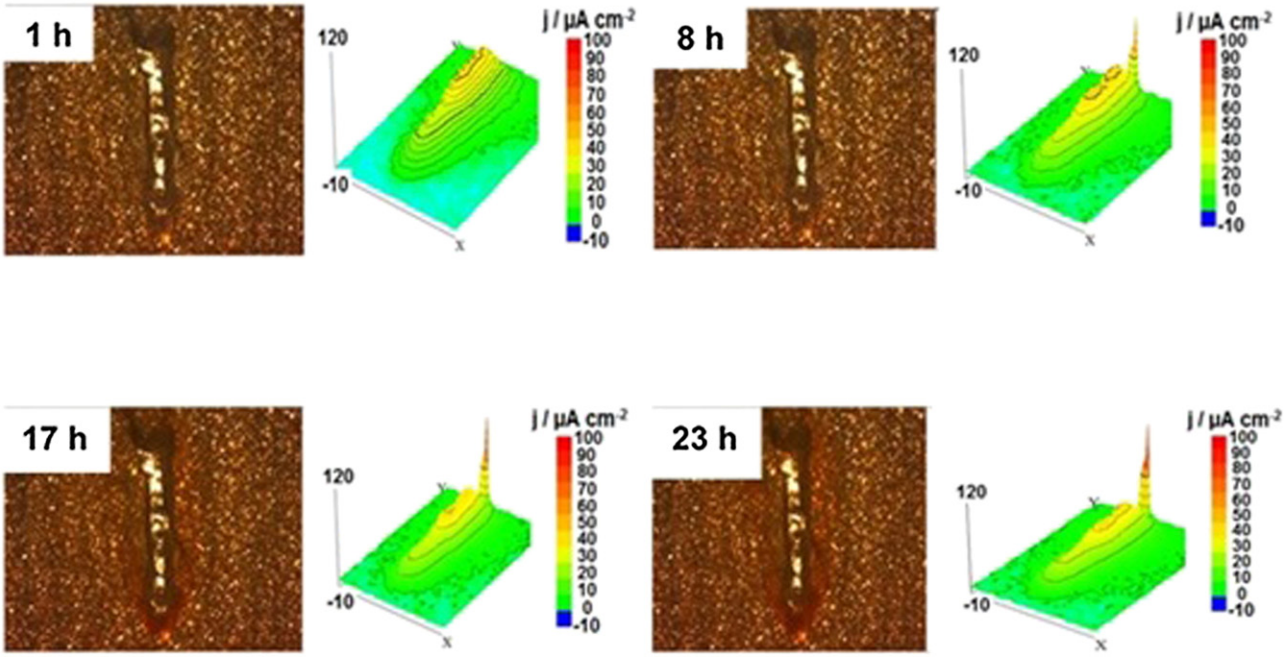

Fig. 11. SVET maps of ionic currents measured above the surface of the carbon steel coated with alkyd primer without mesoporous silica and a provoked defect obtained after different immersion times in 0.05 mol/L NaCl.

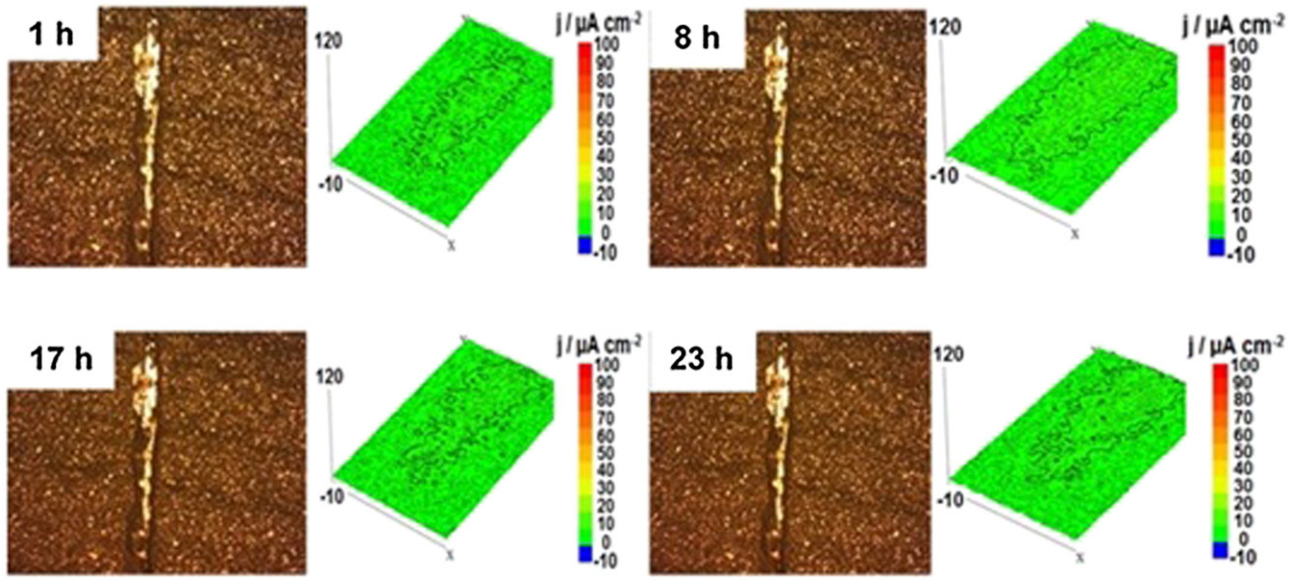

Fig. 12. SVET maps of ionic currents measured above the surface of the carbon steel coated with alkyd primer doped with 15 wt.% of mesoporous silica loaded with dodecylamine inhibitor and a provoked defect obtained after different immersion times in 0.05 mol/L NaCl.

capacitive component was replaced by a constant phase element (CPE), which simulates deviations from a non-ideal capacitor behavior. Fig. 10 illustrates the equivalent circuits used to fit impedance data of immersed samples during 8 h in 0.01 mol/L NaCl and with a provoked defect. Fig. 10a shows the first electrical circuit model used to fit EIS data. The first fitting results have shown a CPE_{dl} exponent value for the three defective samples around 0.5 which is attributed to diffusion controlled process. This is an indication of the need of considering the existence of Warburg resistance in the previous tested equivalent electric circuit model. The final equivalent electric circuit used to fit EIS data is shown in Fig. 10b. The circuit parameters determined after fitting were put together in Table 1.

The fitted data and circuit parameters obtained by the Zview2 software attribution to each of the equivalent electric circuit element is presented in Table 1. The fitting errors are low for most of the parameters and acceptable for others, which means that the chosen equivalent circuit (Fig. 10b) is adequate. As can be seen in Table 1 the value of R_{ct} (charge transfer resistance) for the defective coated sample containing inhibitor-loaded mesoporous silica was 13,661 kΩ $cm^{2,}$ while it was 292.1 kΩ cm^2 and 26.8 kΩ cm^2 for the coated samples containing empty mesoporous silica without inhibitor and alkyd primer without mesoporous silica, respectively. This higher value of R_{ct} for the coated samples with alkyd primer doped with NCs containing corrosion inhibitor indicates a better performance due to the action of dodecylamine

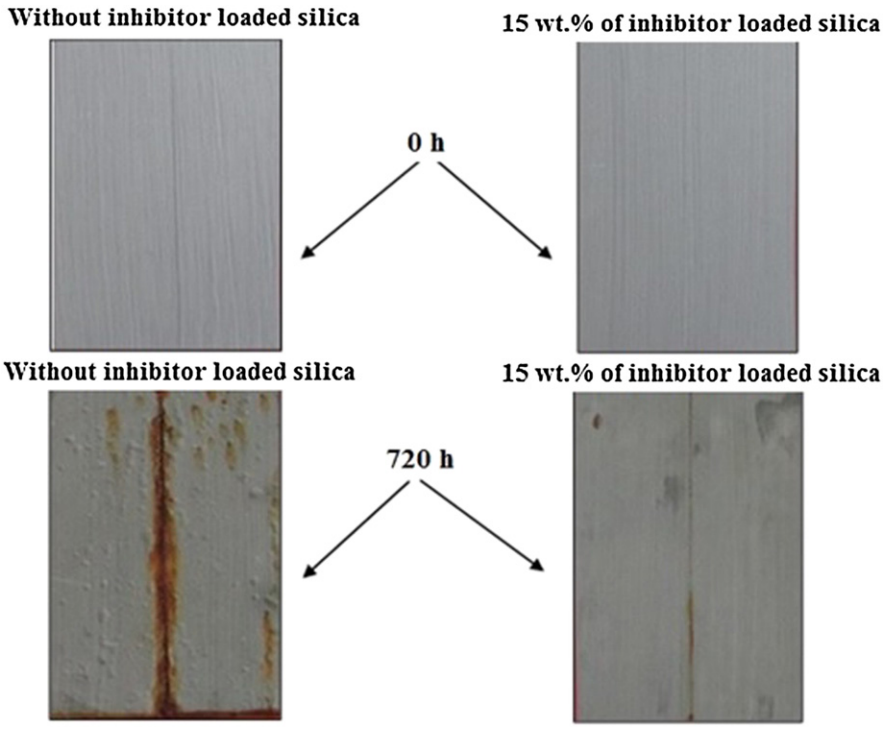

Fig. 13. Aspect of coated samples with two layers of alkyd paint with a primer containing 0 wt.% or 15 wt.% of mesoporous silica before and after 720 h of exposure in the salt spray chamber.

inhibitor that is released from the internal channels of mesoporous silica on the provoked defect. Another information observed in Table 1 are the values of coating resistance, R_{coat}, where the alkyd primer coated samples with inhibitor-loaded NCs presented the highest value (415.7 kΩ cm^2) in comparison to other samples (106.5 kΩ cm^2 for alkyd primer coated samples with empty NCs and 74.8 kΩ cm^2 for pure alkyd primer coated samples), what means that addition of the inhibitor-loaded mesoporous silica increases the barrier properties of the coating. This happens because the particles are very small and in the size range of inert charges or pigments frequently used in paints. The overall analysis reveals that an alkyd paint that is not intrinsically very corrosion resistant can be transformed in a considerably resistant coating when doped with dodecylamine-loaded mesoporous silica.

3.6.2. Scanning vibrating electrode technique (SVET) measurements

SVET measurements for carbon steel coated with two layers of alkyd paint with the primer without mesoporous silica and exposed in 0.05 mol/L NaCl for different immersion times (1 h, 8 h, 17 h and 23 h) are shown in Fig. 11. There is one peak with anodic current density of 46 μA/cm^2 after the first hour of immersion that increases during whole experiment until reaching anodic current density value of 123 μA/cm^2 (after 23 h of immersion). This anodic activity can be observed around the defect and is confirmed by the accumulation of corrosion products on scratched area.

SVET results for carbon steel coated with two layers of alkyd paint with the primer containing 15 wt.% of mesoporous silica are shown in Fig. 12. Results revealed a radically different behavior compared to the coating without mesoporous silica (Fig. 11). The anodic current density was negligible and remains almost constant during 23 h of immersion (5–7 μA/cm^2). These results show an inhibition of the corrosion process due to the action of dodecylamine inhibitor that is released from the internal channels of mesoporous silica caused by pH changes on the damaged area [23,24,35–37]. The effect of dodecylamine corrosion inhibitor is based on the formation of a film adsorbed on the metal surface, which acts as a physical barrier blocking the contact of the metal with the aggressive solution, in a similar way found by other researchers [38].

Another promising future work could be the monitoring of local pH changes on provoked defects in panels of carbon steel coated with alkyd primer doped with dodecylamine-loaded SBA-15 mesoporous silica using the scanning ion-selective electrode technique, SIET.

3.7. Salt spray tests

Fig. 13 presents the results obtained for the salt spray tests for exposure periods of 0 h and 720 h. In these images, it is possible to see that after 720 h the coated samples not doped with mesoporous silica present a strong attack of corrosion in different zones and especially around provoked defect, besides an intense blistering under the coating, which indicates a permeation of the aggressive solution towards metal surface through the defect provoked by the sharp tool. Therefore, it is possible to conclude that the addition of 15 wt.% of mesoporous silica into the primer coating provided an additional protection against corrosion of carbon steel, and after 720 h of exposure there was less corrosion products and blistering around defect area.

4. Conclusions

SBA-15 silica particles with a fibrous structure and mesoporosity has been successfully demonstrated. The encapsulation of dodecylamine in the synthesized mesoporous silica particles was well succeeded.

The incorporation of loaded SBA-15 mesoporous silica in an alkyd primer was also successful. The addition of mesoporous silica alone increased slightly the barrier properties of alkyd primer and the dodecylamine-loaded silica blocked the defects and improved significantly its physical barrier properties allowing the release of the encapsulated inhibitor. A significant increase of the active anticorrosion properties and self-healing were demonstrated and confirmed by EIS and SVET techniques.

The salt spray tests showed clearly that the addition of mesoporous silica on the primer of coated samples provided self-healing properties.

Therefore, an alkyd primer can be transformed in a very resistant coating when doped with dodecylamine-loaded mesoporous silica nanocontainers.

Funding

Authors would like to express sincere gratitude to CNPq — Conselho Nacional de Desenvolvimento Científico e Tecnológico for the scholarship as financial support to develop this research (Process n° 141051/2010-08).

References

[1] S.V. Lamaka, D. Shchukin, D.V. Andreeva, M.L. Zheludkevich, H. Möhwald, M.G.S. Ferreira, Sol–gel/polyelectrolyte active corrosion protection system, Adv. Funct. Mater. 18 (2008) 3137–3147.
[2] D. Shchukin, H. Möhwald, Smart nanocontainers as depot media for feedback active coatings, Chem. Commun. 47 (2011) 8730–8739.
[3] M.F. Montemor, D.V. Snihirova, M.G. Taryba, S.V. Lamaka, I.A. Kartsonakis, I.A.C. Balaskas, G.C. Kordas, J. Tedim, A. Kuznetsova, M.L. Zheludkevich, M.G.S. Ferreira, Self-healing ability in protective coatings modified with combinations of layered double hydroxides and cerium molybdate nanocontainers filled with corrosion inhibitors, Electrochim. Acta 60 (2012) 31–40.
[4] D. Shchukin, S.V. Lamaka, K.A. Yasakau, M.L. Zheludkevich, M.G.S. Ferreira, H. Möhwald, Active anticorrosion coatings with halloysite nanocontainers, J. Phys. Chem. C 112 (2008) 958–964.
[5] D. Fix, D.V. Andreeva, D. Shchukin, H. Mohwald, Application of inhibitor-loaded halloysite nanotubes in active-corrosive coatings, Adv. Funct. Mater. 19 (2009) 1720–1727.
[6] E. Abdullayev, Y. Lvov, Clay nanotubes for corrosion inhibitor encapsulation: release control with end stoppers, J. Mater. Chem. 20 (2010) 6681–6687.
[7] J. Tedim, M.L. Zheludkevich, A.N. Salak, A. Linsekov, M.G.S. Ferreira, Nanostructured LDH-container layer with active protection functionality, J. Mater. Chem. 21 (2011) 15464–16687.
[8] M.L. Zheludkevich, S.K. Poznyak, M.L. Rodrigues, D. Raps, T. Hack, L.F. Dick, T. Nunes, M.G.S. Ferreira, Active protection coatings with layered double hydroxides nanocontainers of corrosion inhibitor, Corros. Sci. 52 (2010) 602–611.
[9] M.F. Montemor, Functional and smart coatings for corrosion protection: a review of recent advances, Surf. Coat. Technol. 258 (2014) 17–37.
[10] J. Tedim, S.K. Poznyak, A. Kuznetsova, D. Raps, T. Hack, M.L. Zheludkevich, M.G.S. Ferreira, Enhancement of active corrosion protection via combination of inhibitor-loaded nanocontainers, ACS Appl. Mater. Interfaces 2 (2010) 1528–1535.
[11] V. Meynen, P. Cool, E.F. Vansant, Verified syntheses of mesoporous materials, Microporous Mesoporous Mater. 125 (2009) 170–223.
[12] T.W. Kim, I.I. Slowing, P.W. Chung, V.S. Lin, Ordered mesoporous polymer–silica hybrid nanoparticles as vehicles for the intracellular controlled release of macromolecules, ACS Nano 5 (2011) 360–366.
[13] S. Shen, P.S. Chow, F. Chen, R.B.H. Tan, Submicron particles of SBA-15 modified with MgO as carriers for controlled drug delivery, Chem. Pharm. Bull. 55 (2007) 985–991.
[14] I. Ben Shir, S. Kababya, T. Amitay-Rosen, Y.S. Balazs, A. Schmidt, Molecular level characterization of the inorganic–bioorganic interface by solid state NMR: alanine on a silica surface, a case study, J. Phys. Chem. B. 114 (2010) 5989–5996.
[15] Z. Tao, Y. Xie, J. Goodisman, T. Asefa, Isomer-dependent adsorption and release of cis- and trans-platin anticancer drugs by mesoporous silica nanoparticles, Langmuir 26 (2010) 8914–8924.
[16] M. Vallet-Regí, M. Manzano, J.M. González-Calbet, E. Okunishid, Evidence of drug confinement into silica mesoporous matrices by STEM spherical aberration corrected microscopy, Chem. Commun. 46 (2010) 2956–2958.
[17] D. Zhao, J. Feng, Q. Huo, N. Melosh, G.H. Fredrickson, B.F. Chmelka, B.F. Stucky, Triblock copolymer syntheses of mesoporous silica with periodic 50 to 300 Angstrom pores, Sci. 279 (1998) 548–552.
[18] G.M. Dhar, G.M. Kumaran, M. Kumar, K.S. Rawat, L.D. Sharma, B.D. Raju, K.S. Rama Rao, Physico-chemical characterization and catalysis on SBA-15 supported molybdenum hydrotreating catalysis, Catal. Today 99 (2005) 309–314.
[19] C.H. Ko, R. Ryoo, Characterization of the porous structure of SBA-15, Chem. Mater. 12 (2000) 1961–1968.
[20] J.P. Thielemann, F. Girgsdies, R. Schlogl, C. Hess, Beilstein, Pore structure and surface area of silica SBA-15: influence of washing and scale-up, J. Nanotechnol. 2 (2011) 110–118.
[21] A. Kiwilsza, J. Mielcarek, A. Pajzderska, J. Wasicki, Ordered mesoporous silica material SBA-15: loading of new calcium channel blocker — lacidipine, J. Microencapsul. 30 (2013) 21–27.
[22] X. Jiang, Y.B. Jiang, N. Liu, H. Xu, S. Rathod, P. Shah, C.J. Brinker, Controlled release from core–shell nanoporous silica particles for corrosion inhibition of aluminum alloys, Nanomater. 2011 (2011) 1–10.

[23] E.V. Skorb, D. Fix, D.V. Andreeva, H. Möhwald, D. Shchukin, Surface-modified mesoporous SiO_2 containers for corrosion protection, Adv. Funct. Mater. 19 (2009) 2373–2379.
[24] D. Borisova, H. Möhwald, D.G. Shchukin, Mesoporous silica nanoparticles for active corrosion protection, ACS Nano 5 (2011) 1939–1946.
[25] T. Chen, J. Fu, pH-responsive nanovalves base on hollow mesoporous silica spheres for controlled release of corrosion inhibitor, J. Nanotech. 23 (2012) 1–8.
[26] M. Yeganeh, M. Saremi, H. Rezaeyan, Corrosion inhibition of steel using mesoporous silica nanocontainers incorporated in the polypyrrole, Prog. Org. Coat. 77 (2014) 1428–1435.
[27] C.A. Gonzalez, R.C. Silva, C. Menchaca, S.S. Guzman, J. Uruchurtu, Use of the silica tubes as nanocontainers for corrosion inhibitor storage, J. Nanotechnol. 2011 (2011) 1–9.
[28] R.R. Price, B.P. Gaber, Y. Lvov, In-vitro release characteristics of tetracycline HCl, khellin and nicotinamide adenine dinucleotide from halloysite; a cylindrical mineral, J. Microencapsul. 18 (2001) 713–722.
[29] S. Brunauer, P.H. Emmett, E. Teller, Adsorption of gases in multimolecular layers, J. Am. Chem. Soc. 60 (1938) 309–319.
[30] M.C. Chao, H.P. Lin, H.S. Sheu, C.Y. Mou, A study of morphology of mesoporous silica SBA-15, Stud. Surf. Sci. Catal. 141 (2002) 387–394.
[31] A. Katijar, S. Yadav, P.G. Smirniots, N.G. Pinto, Syntheses of ordered large pore SBA-15 spherical particles for adsorption of biomolecules, J. Chromatogr. A 1122 (2006) 13–20.
[32] T. Chen, J. Fu, An intelligent anticorrosion coating based on pH-responsive supramolecular nanocontainers, J. Nanotechnol. 23 (2012) 1–12.
[33] D. Borisova, D. Akçakayairan, M. Shenderlein, H. Möhwald, D.G. Shchukin, Nanocontainer-based anticorrosive coatings: effect of the container size on the self-healing performance, Mat. View 23 (2013) 3799–3812.
[34] M.L. Zheludkevich, D. Shchukin, K.A. Yasakau, H. Möhwald, M.G.S. Ferreira, Anticorrosion coatings with self-healing effect based on nanocontainers impregnated with corrosion inhibitor, Chem. Mater. 19 (2007) 402–411.
[35] D. Borisova, H. Möhwald, D.G. Shchukin, Influence of embedded nanocontainers on the efficiency of active anticorrosion coatings for aluminum alloys part I: influence of nanocontainers concentration, ACS Appl. Mater. Interfaces 4 (2012) 2931–2939.
[36] Z. Zheng, X. Huang, M. Schenderlien, D. Borisova, R. Cao, H. Möhwald, D.G. Shchukin, Self-healing and antifouling multifunctional coatings based on pH and sulfide ion sensitive nanocontainers, Mater. Views. 23 (2013) 3307–3314.
[37] F. Maia, J. T, A.D. Lisenkov, A.N. Salak, M.L. Zheludkevich, M.G.S. Ferreira, Silica nanocontainers for active corrosion protection, R. Soc. Chem. Adv. 4 (2012) 1287–1298.
[38] J.M. Bastidas, J.L. Polo, E. Cano, Substitutional inhibition mechanism of mild steel hydrochloric acid corrosion by hexylamine and dodecylamine, J. Appl. Electrochem. 30 (2000) 1173–1177.